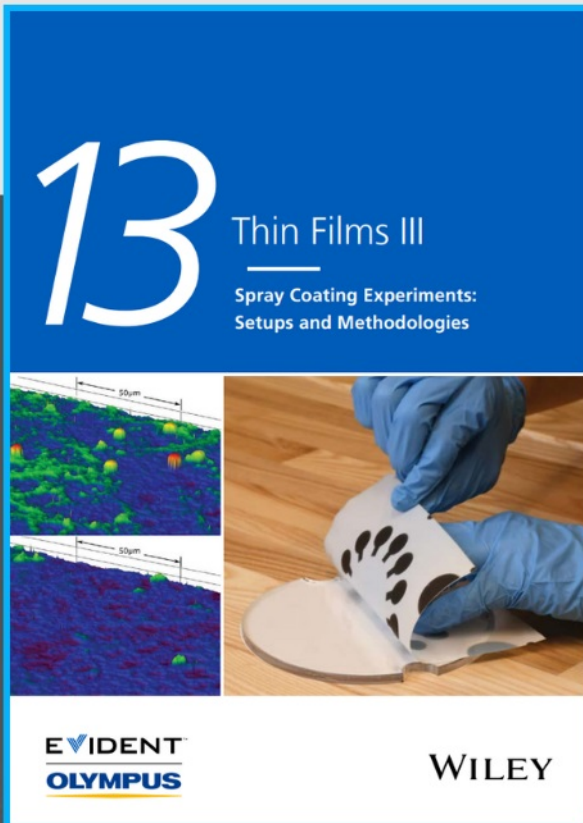




# Spray Coating Experiments: Setups and Methodologies



**The latest eBook from  
Advanced Optical Metrology.  
Download for free.**

*Spray Coating Experiments: Setups and Methodologies*, is the third in our Thin Films eBook series. This publication provides an introduction to spray coating, three article digests from Wiley Online Library and the latest news about Evident's Image of the Year Award 2022.

Wiley in collaboration with Evident, are committed to bridging the gap between fundamental research and industrial applications in the field of optical metrology. We strive to do this by collecting and organizing existing information, making it more accessible and useful for researchers and practitioners alike.

**EVIDENT**  
**OLYMPUS**

**WILEY**

# Polarization-Independent Second Harmonic Generation in 2D Van Der Waals Kagome Nb<sub>3</sub>SeI<sub>7</sub> Crystals

Yuqiang Fang, Xin Feng, Dong Wang, Yang Ding, Tianquan Lin, Tianyou Zhai,\* and Fuqiang Huang\*

Second harmonic generation (SHG) of 2D crystals has been of great interest due to its advantages of phase-matching and easy integration into nanophotonic devices. However, the polarization-dependence character of the SHG signal makes it highly troublesome but necessary to match the laser polarization orientation relative to the crystal, thus achieving the maximum polarized SHG intensity. Here, it is demonstrated a polarization-independent SHG, for the first time, in the van der Waals Nb<sub>3</sub>SeI<sub>7</sub> crystals with a breathing Kagome lattice. The Nb<sub>3</sub> triangular clusters and Janus-structure of each Nb<sub>3</sub>SeI<sub>7</sub> layer are confirmed by the STEM. Nb<sub>3</sub>SeI<sub>7</sub> flake shows a strong SHG response due to its noncentrosymmetric crystal structure. More interestingly, the SHG signals of Nb<sub>3</sub>SeI<sub>7</sub> are independent of the polarization of the excitation light owing to the in-plane isotropic arrangement of nonlinear active units. This work provides the first layered nonlinear optical crystal with the polarization-independent SHG effect, providing new possibilities for nonlinear optics.

as the basic frequency conversion, self-referencing of frequency combs, optical atomic clocks, and the emerging all-optical quantum computing.<sup>[1–9]</sup> In practice, when the nonlinear optical crystals are excited by the linear-polarized lasers, the generated second harmonic generation (SHG) signal intensity is highly dependent on the angles between polarized light and crystal axis, which results from the anisotropy of the intrinsic second-order polarizability tensor  $\chi^{(2)}$ .<sup>[10–11]</sup> For example, the polarization-dependent SHG plot for the 3R-MoS<sub>2</sub> shows a six-fold petal shape.<sup>[12–14]</sup> In such cases, filtering or modulating the SHG signals to achieve the polarized-SHG with maximum intensity has been a huge hassle in a specific application scenario, given that linear-polarized SHG signals are preferred in the modulation and processing of optical signals.

Compared to fabricating complicated optical systems or designing plasmonic nanostructure,<sup>[15–17]</sup> achieving the polarization-independent SHG response directly from nonlinear crystals has been an aspirational approach, but such compound remains undiscovered yet.

Kagome semiconductor Nb<sub>3</sub>I<sub>8</sub> has a layered CdI<sub>2</sub> structure with one-quarter of the octahedral Nb vacancies.<sup>[18]</sup> The arrangements of occupied Nb atoms lead to the Nb<sub>3</sub> triangles with one capping iodine ion. The one unpaired electron of Nb<sub>3</sub> cluster and Kagome lattice endows Nb<sub>3</sub>I<sub>8</sub> with intriguing physical properties, such as topological flat bands, 2D magnetism, and large spontaneous valley polarization.<sup>[19–22]</sup> According to the topological charge stabilization rule, more electronegative elements prefer to occupy the electron-rich sites.<sup>[23–24]</sup> Therefore, the less electronegative chalcogenides (S, Se, and Te) can replace the lower electron-density capping iodine ion, which results in the formation of Nb<sub>3</sub>I<sub>7</sub>X (X = S, Se, Te). Compared to Nb<sub>3</sub>I tetrahedron, Nb<sub>3</sub>X has a larger dipole moment. The unidirectionally oriented Nb<sub>3</sub>X tetrahedral dipoles lead to 2D ferroelectric behavior of layered Nb<sub>3</sub>I<sub>7</sub>X, whereas alternating Nb<sub>3</sub>X dipoles give an antiferroelectric structure. Moreover, Nb<sub>3</sub>I<sub>7</sub>X could show novel nonlinear optical properties due to the in-plane isotropic arrangement of nonlinear optical active units.

Here, we have successfully synthesized Nb<sub>3</sub>SeI<sub>7</sub> crystals by a chemical vapor transport method using iodine. The single crystal X-ray diffraction reveals that Nb<sub>3</sub>SeI<sub>7</sub> crystallizes in a noncentrosymmetric space group *P6<sub>3</sub>mc*. The Janus structure and breathing Kagome lattice are verified by scanning transmission electron microscopy. Nb<sub>3</sub>SeI<sub>7</sub> has a band gap of 1.54 eV,

## 1. Introduction

Second-order nonlinear optics has been a cornerstone in a large number of classical and quantum applications, such

Y. Fang, F. Huang

State Key Laboratory of High-Performance Ceramics and Super fine Microstructure

Shanghai Institute of Ceramics

Chinese Academy of Sciences

Shanghai 200050, P. R. China

E-mail: huangfq@mail.sic.ac.cn

X. Feng, T. Zhai

State Key Laboratory of Material Processing and Die & Mold Technology

School of Materials Science and Technology

Huazhong University of Science and Technology

Wuhan 430074, P. R. China

E-mail: zhaity@hust.edu.cn

D. Wang, Y. Ding

Center for High-Pressure Science and Technology Advanced Research

Beijing 100094, P. R. China

T. Lin

School of Materials Science and Engineering

Shanghai Jiao Tong University

Shanghai 200240, P. R. China

F. Huang

State Key Laboratory of Rare Earth Materials Chemistry and Applications

College of Chemistry and Molecular Engineering

Peking University

Beijing 100871, P. R. China

 The ORCID identification number(s) for the author(s) of this article can be found under <https://doi.org/10.1002/smll.202207934>.

DOI: 10.1002/smll.202207934

and it shows SHG response in the wavelength ranging from 800 to 1020 nm. More interestingly,  $\text{Nb}_3\text{SeI}_7$  shows polarization-independent SHG signals in perpendicular and parallel polarization configurations under the excitation light at 820, 860, and 900 nm for the first time.

## 2. Results and Discussion

Bulk  $\text{Nb}_3\text{SeI}_7$  crystallizes in a hexagonal space group  $P6_3mc$  with lattice parameters of  $a = 7.564 \text{ \AA}$  and  $c = 13.654 \text{ \AA}$ . The detailed crystallographic information can be seen in Table S1–S4, Supporting Information.<sup>[25]</sup> Figure 1A shows that  $\text{Nb}_3\text{SeI}_7$  has a van der Waals (vdW) layered structure stacked by Janus  $\text{Nb}_3\text{SeI}_7$  layers, in which Nb atoms are sandwiched between the I and I-Se atomic layers. Anionic layer stacking mode is (...ABCBA...), and adjacent layers are related by a  $6_3$ -screw axis. Each Nb atom is coordinated by five I atoms, one Se atom, and two Nb atoms. Nb–I bond lengths are 2.73  $\text{\AA}$ , 2.92  $\text{\AA}$ , and 3.03  $\text{\AA}$ , and Nb–Se bond length is 2.56  $\text{\AA}$ , respectively. The three Nb atoms are displaced from the octahedral central sites toward each other, resulting in the formation of trinuclear  $\text{Nb}_3$  clusters. The alternate Nb triangles with Nb–Nb distances of 3.01  $\text{\AA}$  and 4.58  $\text{\AA}$  form a breathing Kagome lattice, as shown in Figure 1B. The  $\text{Nb}_3$  clusters are capped by the Se atoms, and all the  $\text{Nb}_3\text{Se}$  tetrahedra are oriented in the

same direction throughout the crystal structure, which breaks the central symmetry.

To further confirm the atomic configurations of Janus structure and Kagome lattice for  $\text{Nb}_3\text{SeI}_7$  crystal, scanning transmission electron microscopy (STEM) was carried out. The cross-sectional STEM high-angle annular dark-field (HAADF) image reveals that the  $\text{Nb}_3\text{SeI}_7$  monolayer consists of one layer of Nb atoms sandwiched between two layers of I and I–Se atoms (Figure 1C). To distinguish the distribution of Se and I atoms in a quantitative way, the line profiles of intensity were plotted across the STEM image of two atomic layers (Figure S1, Supporting Information). The blue curve shows the same intensity of I atoms, whereas the periodic fluctuating intensity in the red line indicates the existence of Se–I atomic layers. This can reveal the Janus structure of monolayer  $\text{Nb}_3\text{SeI}_7$ . Figure 1D shows the STEM-HAADF image of (001) plane for the  $\text{Nb}_3\text{SeI}_7$  crystal. Because  $\text{Nb}_3\text{SeI}_7$  layers take an ABAB stacking mode, the triangular  $\text{Nb}_3$  clusters of various layers overlap each other to form a six-pointed star, consistent with the atomic configuration of its single crystal structure. The selected area electron diffraction (SAED) from [001] direction reveals the diffraction spots indexed as (–120) and (010) lattice planes (Figure S2, Supporting Information). Moreover, the energy-dispersive X-ray spectroscopy mapping shows that the Nb, Se, and I elements are distributed uniformly with the atomic ratio of 1: 0.3: 2.3. (Figure S3, Supporting Information)

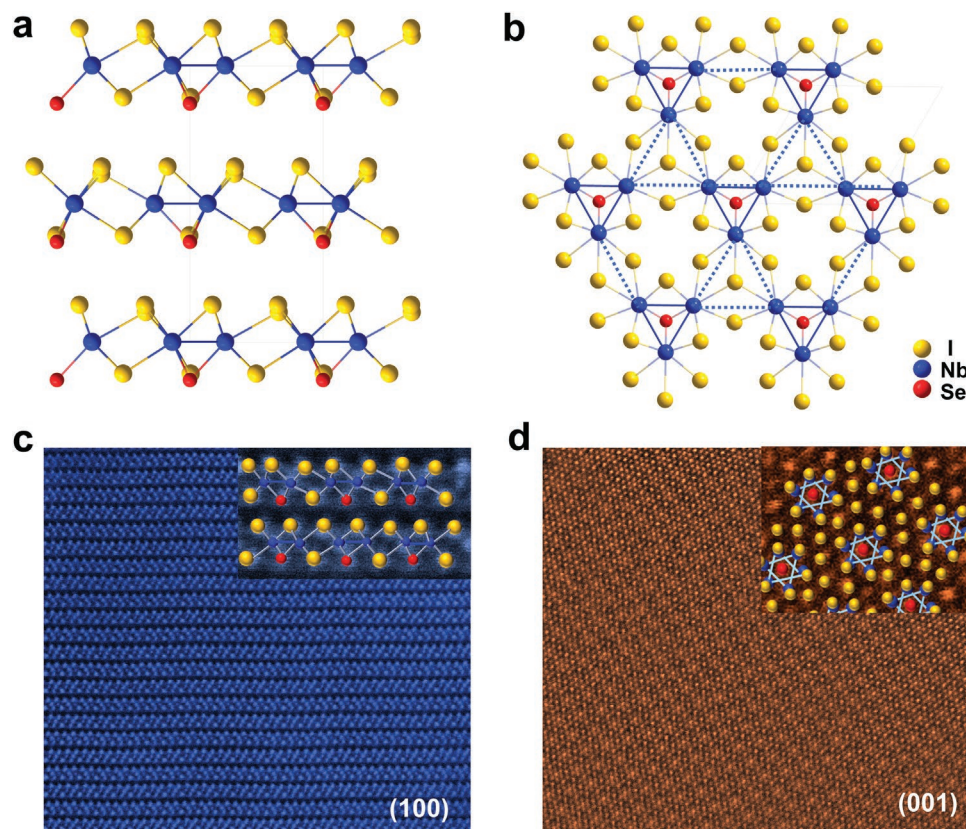


**Figure 1.** Crystal structure and STEM characterization of  $\text{Nb}_3\text{SeI}_7$ . a) Side view of  $\text{Nb}_3\text{SeI}_7$  showing a Janus structure, where the blue, yellow, and red spheres represent Nb, I, and Se, respectively. b) Top view of monolayer  $\text{Nb}_3\text{SeI}_7$  showing a breathing Kagome lattice. c) Atomic-resolution STEM-HAADF image of (100) lattice plane for  $\text{Nb}_3\text{SeI}_7$  crystal. d) STEM-HAADF image of (001) lattice plane.

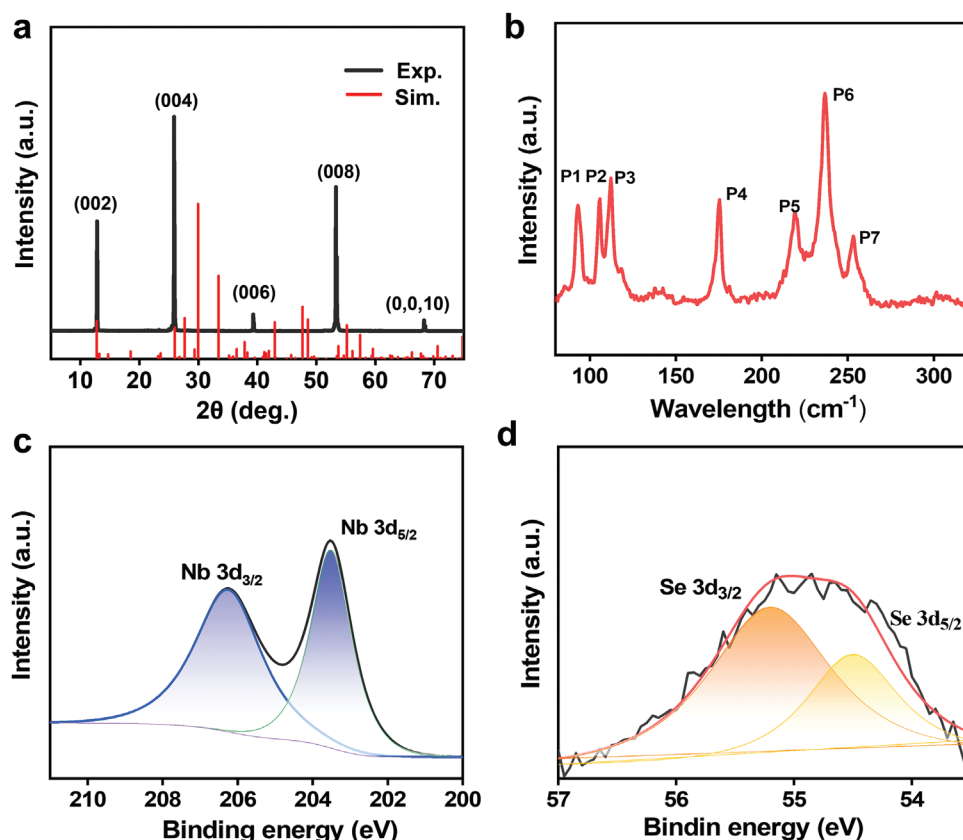


**Figure 2.** a) Experimental and simulated XRD pattern of  $\text{Nb}_3\text{Se}_7$  crystals. b) Raman spectrum of  $\text{Nb}_3\text{Se}_7$  sample. c,d) High-resolution Nb 3d and Se 3d XPS spectra.

The powder X-ray diffraction pattern of the  $\text{Nb}_3\text{Se}_7$  single crystal matches well with the simulated peaks from the resolved single crystal structure, indicating high purity and crystallinity of the  $\text{Nb}_3\text{Se}_7$  crystals (Figure 2A). The room-temperature Raman spectrum of the  $\text{Nb}_3\text{Se}_7$  crystal shows seven characteristic peaks located at 93, 106, 112, 176, 220, and 237  $\text{cm}^{-1}$ , respectively (Figure 2B). In addition, X-ray photoelectron spectroscopy (XPS) was performed to detect the various bonding states of Nb and Se atoms in  $\text{Nb}_3\text{Se}_7$  crystals (Figure 2C,D, Supporting Information). The Se spectra show  $3d_{3/2}$  and  $3d_{5/2}$  peaks at 55.2 and 54.5 eV, indicating a valence state of  $-2$ . The characteristic Nb  $3d_{3/2}$  and  $3d_{5/2}$  peaks located at 206.2 eV and 203.5 eV are the same as that of  $\text{NbN}$ ,<sup>[25]</sup> which confirms that the valence state of Nb is  $+3$ .

The bandgap of  $\text{Nb}_3\text{Se}_7$  crystal was determined through the micro-optical absorption measurement in wavelengths ranging from 600 to 1100 nm. Figure 3A shows the absorption spectra of the  $\text{Nb}_3\text{Se}_7$  flake, revealing a band gap of 1.54 eV. Compared with  $\text{Nb}_3\text{I}_8$  with a band gap of 1.0 eV, the larger band gap of  $\text{Nb}_3\text{Se}_7$  is caused by the decreased electron density of Nb 4d orbitals after the substitution of I atoms by Se atoms. In addition, the introduction of Se ion in capping I sites can change the layer stacking mode and increase the dipole moment. SHG measurements were performed to investigate the nonlinear optical properties of  $\text{Nb}_3\text{Se}_7$  crystals.

Figure 3B shows the strong SHG signals of  $\text{Nb}_3\text{Se}_7$  flakes under excitation wavelengths ranging from 800 to 1020 nm.

The SHG peaks appear at half of the excitation wavelength and the maximum peak is located at 430 nm. To further confirm the contribution of signals originating from SHG, the SHG response was measured under various excitation power ranging from 10 to 40 mW (Figure 3C). The power dependence of SHG intensity was plotted in logarithmic coordinates. The curve can be fitted by a power-law function with a slope of 2.1, which is close to the theoretical value of 2 for SHG.<sup>[26]</sup> Figure 3D shows the robust SHG signals of  $\text{Nb}_3\text{Se}_7$  flake measured at temperatures ranging from 343 to 543 K, indicating its potential for high-temperature application.

The polarization dependence of SHG intensity in the  $\text{Nb}_3\text{Se}_7$  flake was characterized. The sample was rotated from 0 to 180° with a step of 15° with excitation polarization fixed, then the collected SHG signals reveal the nonlinear response at various polarization angles. Figure S4, Supporting Information shows the polar plots of wavelength-dependent SHG intensities under the parallel and perpendicular polarization configuration. The intensity under the parallel polarization is larger than that of perpendicular polarization under the excitation light below 440 nm. Figure 4A,C, Supporting Information shows near-circular SHG intensity plots at the excitation light of 820, 860, and 900 nm under parallel and perpendicular polarization configurations. Impressively, the SHG response of  $\text{Nb}_3\text{Se}_7$  is nearly independent of the polarization of incident light as the SHG intensities are almost constant for various angle measurements. This polarization-independence SHG phenomenon has

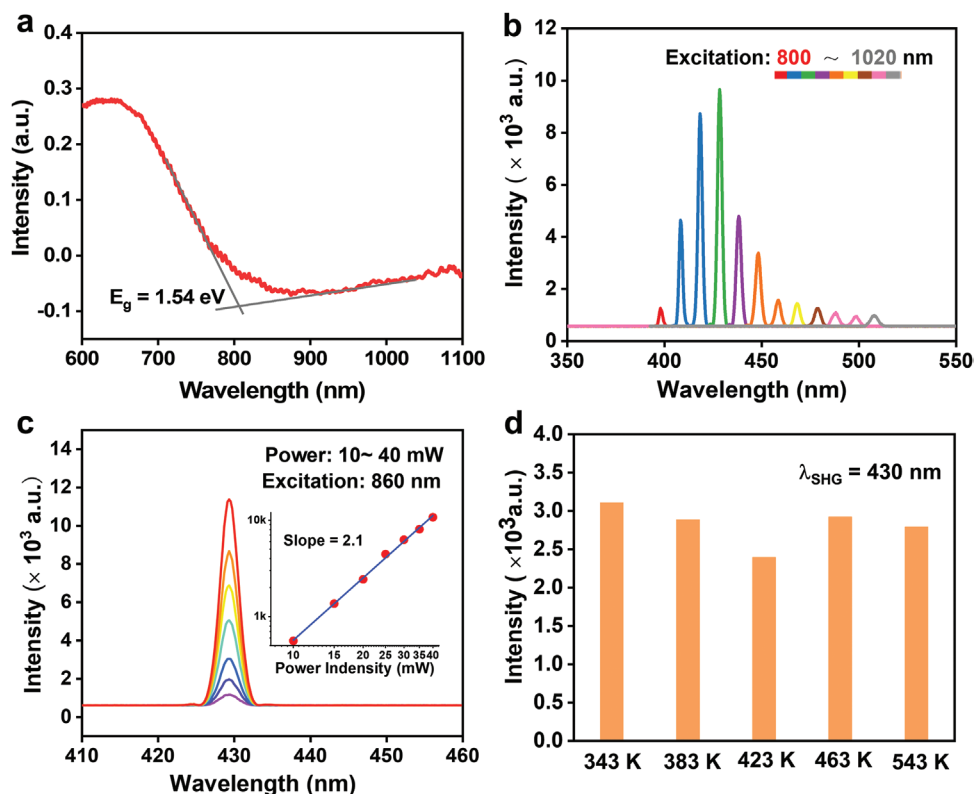


**Figure 3.** a) Optical absorption of  $\text{Nb}_3\text{Se}_7$  flake. b) SHG signals of a  $\text{Nb}_3\text{Se}_7$  flake under different excitation wavelengths ranging from 800 to 1020 nm. c) SHG spectra in the incident light of 860 nm with power from 10 to 40 mW. Inset: Power-dependent SHG intensity. d) SHG signals were measured at temperatures from 343–543 K.

been realized in plasmonic nanostructures, such as the hexagonal gold nanoparticle array, multiarmed trapezoidal antenna, and oligomer clusters.<sup>[15–17]</sup> The in-plane isotropy of these systems assembled with NLO units leads to their SHG response independence from the polarized incident light.

However, for an inorganic compound, the generated SHG signal is always anisotropic which is normally decided by the crystal symmetry and orientation.<sup>[27–29]</sup> For example, monolayer  $\text{MoS}_2$  has a  $D_{3h}$  point group, resulting in a sixfold symmetry in the polar plot (Figure S5, Supporting Information). With these regards, the polarization-independent SHG of  $\text{Nb}_3\text{Se}_7$  is anomalous, which has not been reported in other compounds yet. Inspired by the arrangement mode of plasmonic structures, we speculate that polarization-independent SHG signals may originate from the in-plane isotropic geometrical configuration of  $\text{Nb}_3\text{Se}$  NLO active units in the breathing Kagome lattice (Figure 4D).

### 3. Conclusion

In summary, we report a vdW layered crystal  $\text{Nb}_3\text{Se}_7$  crystal with a noncentrosymmetric structure.  $\text{Nb}_3\text{Se}_7$  layers featured a Janus structure, and the  $\text{Nb}_3$  clusters form the breathing Kagome lattice, as confirmed by the HAADF-STEM image.  $\text{Nb}_3\text{Se}_7$  has a band gap of 0.6 eV and shows a significant SHG response. Moreover, the polarized-SHG intensities are not

affected by the polarization of the incident light, which can overcome the limitations of polarization-selective excitation of nonlinear optical crystals. Our work provides a new 2D noncentrosymmetric material for nonlinear optics, ferroelectric, and photo-electronics.

### 4. Experimental Section

**Preparation of  $\text{Nb}_3\text{Se}_7$  Crystals:**  $\text{Nb}_3\text{Se}_7$  crystals were synthesized by a chemical vapor transport method. The reagents Nb (Adamas-beta, 99.9%), Se (Adamas-beta, 99.9%), and I (Adamas-beta, 99.9%) were mixed by a molar ratio of 3: 1: 7. The mixture was sealed in an evacuated silica tube, which was heated in a two-zone tube furnace. The tube was heated to a temperature gradient of 1073 K to 973 K at 3 K/min and held for 5 days. The shiny  $\text{Nb}_3\text{Se}_7$  crystals can be obtained in the cold area of the tube.

**Single Crystal Determination:** Suitable  $\text{Nb}_3\text{Se}_7$  single crystal was chosen to perform the data collection. Single-crystal X-ray diffraction was performed on a Bruker D8QUEST diffractometer equipped with Mo K  $\alpha$  radiation. The diffraction data were collected at room temperature by the  $\omega$ - and  $\varphi$ -scan methods. The crystal structures were solved and refined using APEX3 program. Absorption corrections were performed using the multiscan method.

**Characterization:** The element compositions of  $\text{Nb}_3\text{Se}_7$  crystal were confirmed through energy-dispersive X-ray spectroscopy. The microstructure of the exfoliated  $\text{Nb}_3\text{Se}_7$  flakes was studied by high-resolution transmission electron microscopy. The Raman spectra measurements were carried out on a microscope spectrometer, equipped with  $\times 50$  optical objective and 1800 grooves  $\text{mm}^{-1}$  grating. The excitation

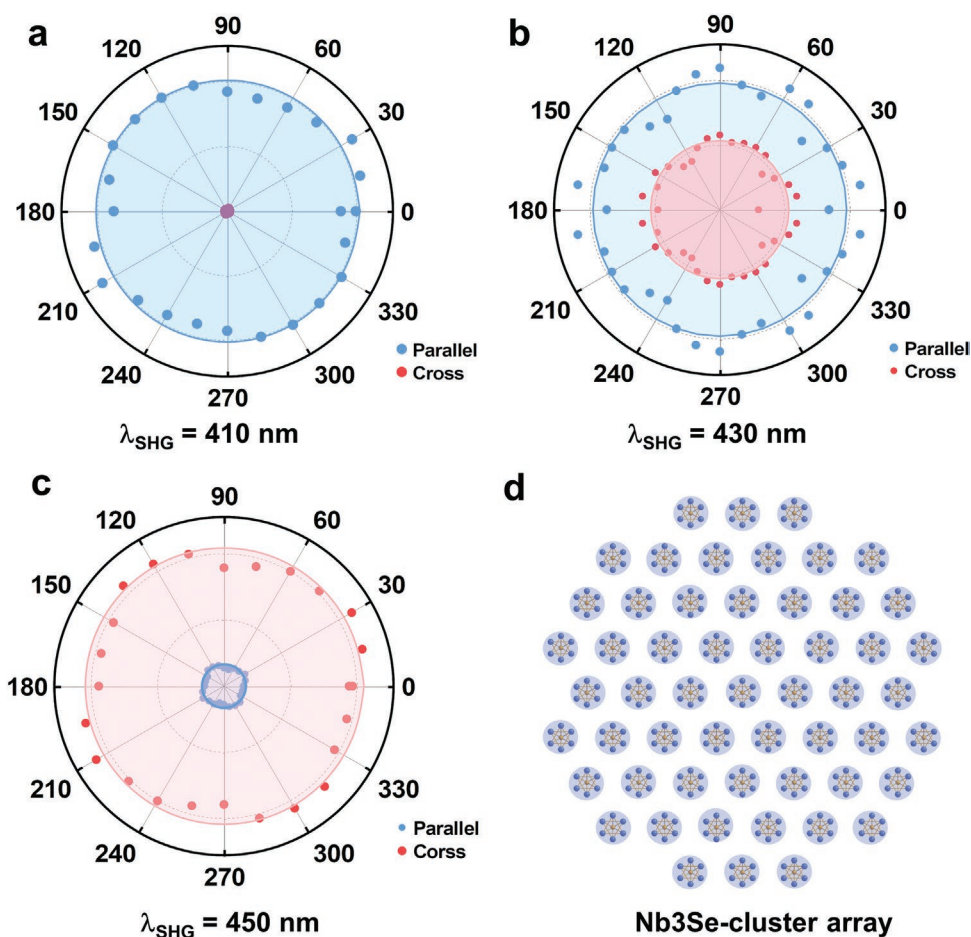


**Figure 4.** Polar plots of the SHG intensities for the  $\text{Nb}_3\text{Se}_7$  flake in perpendicular and parallel polarization configurations under the excitation light at a) 820 nm, b) 860 nm, c) 900 nm. d) Schematic diagram of  $\text{Nb}_3\text{Se}_7$  cluster array.

power and wavelength were 1 mW and 532 nm, respectively. The SHG signals were collected in a chameleon femtosecond laser. To detect the polarized SHG, the incident laser was polarized, and the scattering light was in the direction parallel and perpendicular to the incident light. The optical bandgaps of  $\text{Nb}_3\text{Se}_7$  flakes with different thicknesses were determined by Jasco MSV-5200 microscopic spectrophotometer.

[CCDC 2 221 828 contains the supplementary crystallographic data for this paper. These data can be obtained free of charge from The Cambridge Crystallographic Data Centre via [www.ccdc.cam.ac.uk/data\\_request/cif](http://www.ccdc.cam.ac.uk/data_request/cif).]

## Supporting Information

Supporting Information is available from the Wiley Online Library or from the author.

## Acknowledgements

Y.F. and X.F. contributed equally to this work. This work was supported by financial support from the National Key Research and Development Program of China (Grant No. 2019YFA0210600) and the National Natural Science Foundation of China (Grant No. 52103353, 51922103).

## Conflict of Interest

The authors declare no conflict of interest.

## Data Availability Statement

The data that support the findings of this study are available from the corresponding author upon reasonable request.

## Keywords

polarization-independent second harmonic generation (SHG), 2D kagome compound,  $\text{Nb}_3\text{Se}_7$

Received: December 19, 2022

Revised: February 27, 2023

Published online:

[1] H. Liu, Y. Li, Y. S. You, S. Ghimire, T. F. Heinz, D. A. Reis, *Nat. Phys.* **2017**, *13*, 262.

[2] N. Yoshikawa, T. Tamaya, K. Tanaka, *Science* **2017**, *356*, 736.

- [3] S. Wu, S. Buckley, J. R. Schaibley, L. Feng, J. Yan, D. G. Mandrus, F. Hatami, W. Yao, J. Vučković, A. Majumdar, X. Xu, *Nature* **2015**, *520*, 69.
- [4] Z. Sun, A. Martinez, F. Wang, *Nat. Photonics* **2016**, *10*, 227.
- [5] A. Zumbusch, G. R. Holtom, X. S. Xie, *Phys. Rev. Lett.* **1999**, *82*, 4142.
- [6] B. Corcoran, C. Monat, C. Grillet, D. J. Moss, B. J. Eggleton, T. P. White, L. O'Faolain, T. F. Krauss, *Nat. Photonics* **2009**, *3*, 206.
- [7] X. Lu, G. Moille, A. Rao, D. A. Westly, K. Srinivasan, *Nat. Photonics* **2021**, *15*, 131.
- [8] M. Y. Niu, I. L. Chuang, J. H. Shapiro, *Phys. Rev. Lett.* **2018**, *120*, 160502.
- [9] P. Beaujean, B. Champagne, S. Grimme, M. de Wergifosse, *J. Phys. Chem. Lett.* **2021**, *12*, 9684.
- [10] C. Chen, L. Gao, W. Gao, C. Ge, X. Du, Z. Li, Y. Yang, G. Niu, J. Tang, *Nat. Commun.* **2019**, *10*, 1927.
- [11] N. Bloembergen, *Rev. Mod. Phys.* **1982**, *54*, 685.
- [12] Y. Dong, M.-M. Yang, M. Yoshii, S. Matsuoka, S. Kitamura, T. Hasegawa, N. Ogawa, T. Morimoto, T. Ideue, Y. Iwasa, *Nat. Nanotechnol.* **2022**, *11*, 01252.
- [13] X. Zheng, Y. Wei, X. Zhang, Z. Wei, W. Luo, X. Guo, J. Liu, G. Peng, W. Cai, H. Huang, T. Lv, C. Deng, X. Zhang, *Adv. Funct. Mater.* **2022**, *32*, 2202658.
- [14] J. Shi, P. Yu, F. Liu, P. He, R. Wang, L. Qin, J. Zhou, X. Li, J. Zhou, X. Sui, S. Zhang, Y. Zhang, Q. Zhang, T. C. Sum, X. Qiu, Z. Liu, X. Liu, *Adv. Mater.* **2017**, *29*, 1701486.
- [15] X.-X. Wu, W.-Y. Jiang, X.-F. Wang, L.-Y. Zhao, J. Shi, S. Zhang, X. Sui, Z.-X. Chen, W.-N. Du, J.-W. Shi, Q. Liu, Q. Zhang, Y. Zhang, X.-F. Liu, *ACS Nano* **2021**, *15*, 1291.
- [16] H. Aouani, M. Navarro-Cia, M. Rahmani, T. P. H. Sidiropoulos, M. Hong, R. F. Oulton, S. A. Maier, *Nano Lett.* **2012**, *12*, 4997.
- [17] S.-D. Liu, E. S. P. Leong, G.-C. Li, Y. Hou, J. Deng, J. H. Teng, H. C. Ong, D. Y. Lei, *ACS Nano* **2016**, *10*, 1442.
- [18] B. J. Kim, B. J. Jeong, S. Oh, S. Chae, K. H. Choi, S. S. Nanda, T. Nasir, S. H. Lee, K.-W. Kim, H. K. Lim, L. Chi, I. J. Choi, M.-K. Hong, D. K. Yi, H. K. Yu, J.-H. Lee, J.-Y. Choi, *Phys. Status Solidi RRL* **2019**, *13*, 1800448.
- [19] R. Peng, Y. Ma, X. Xu, Z. He, B. Huang, Y. Dai, *Phys. Rev. B* **2020**, *102*, 035412.
- [20] F. Conte, D. Ninno, G. Cantele, *Phys. Rev. Res.* **2020**, *2*, 033001.
- [21] B. Mortazavi, X. Zhuang, T. Rabczuk, *Appl. Phys. A* **2022**, *128*, 934.
- [22] G. Cantele, F. Conte, L. Zullo, D. Ninno, *Phys. Rev. B* **2022**, *106*, 085418.
- [23] M. Hatanaka, *J. Phys. Chem. A* **2015**, *119*, 1074.
- [24] J.-i. Aihara, *Chem* **1987**, *60*, 2268.
- [25] A. Darlinski, J. Halbritter, *Surf. Interface Anal.* **1987**, *10*, 223.
- [26] R. Beams, L. G. Cançado, S. Krylyuk, I. Kalish, B. Kalanyan, A. K. Singh, K. Choudhary, A. Bruma, P. M. Vora, F. Tavazza, A. V. Davydov, S. J. Stranick, *ACS Nano* **2016**, *10*, 9626.
- [27] Y. Fang, X. Hu, W. Zhao, J. Pan, D. Wang, K. Bu, Y. Mao, S. Chu, P. Liu, T. Zhai, F. Huang, *J. Am. Chem. Soc.* **2019**, *141*, 790.
- [28] Y. Fang, F. Wang, R. Wang, T. Zhai, F. Huang, *Adv. Mater.* **2021**, *33*, 2101505.
- [29] X. Zhou, J. Cheng, Y. Zhou, T. Cao, H. Hong, Z. Liao, S. Wu, H. Peng, K. Liu, D. Yu, *J. Am. Chem. Soc.* **2015**, *137*, 7994.